Proton and Electron Transfer during the Reduction of Molecular Oxygen by Fully Reduced Cytochrome *c* Oxidase: A Flow-Flash Investigation Using Optical Multichannel Detection†

Stefan Paula,‡ Artur Sucheta,§ Istvan Szundi,|| and Ólöf Einarsdóttir*,||

Department of Chemistry and Biochemistry, University of California at Santa Cruz, Santa Cruz, California 95064, Department of Membrane Biochemistry, Max-Planck-Institut for Biochemistry, 82152 Martinsried, Germany, and Department of Radiology, Dartmouth College, HB7785, Vail Building Room 715, Hanover, New Hampshire 03755

Received June 8, 1998; Revised Manuscript Received December 2, 1998

ABSTRACT: Proton and electron transfer events during the reaction of solubilized fully reduced bovine heart cytochrome *c* oxidase with molecular oxygen were investigated using the flow-flash technique. Time-resolved spectral changes resulting from ligand binding and electron transfer events were detected simultaneously with pH changes in the bulk. The kinetics and spectral changes in the visible region (450−750 nm) were probed by optical multichannel detection, allowing high spectral resolution on time scales from 50 ns to 50 ms. Experiments were carried out in the presence and absence of pH-sensitive dyes (carboxyfluorescein at pH 6.5, phenol red at pH 7.5, and *m*-cresol purple at pH 8.5) which permitted separation of spectral changes due to proton transfer from those caused by ligand binding and electron transfer. The transient spectra recorded in the absence of dye were analyzed by singular-value decomposition and multiexponential fitting. Five apparent lifetimes (0.93 μs, 10 μs, 36 μs, 90 μs, and 1.3 ms at pH 7.5) could consistently be distinguished and provided a basis for a reaction mechanism consistent with our most recent kinetic model [Sucheta, A., Szundi, I., and Einarsdóttir, Ó. (1999) *Biochemistry 37*, 17905−17914]. The dye response indicated that proton uptake occurred concurrently with the two slowest electron transfer steps, in agreement with previous results based on single-wavelength detection [Hallén, S., and Nilsson, T. (1992) *Biochemistry 31*, 11853−11859]. The stoichiometry of the proton uptake reactions was approximately 1.3 ± 0.3, 1.4 ± 0.3, and 1.6 ± 0.5 protons per enzyme at pH 6.5, 7.5, and 8.5, respectively. The electron transfer between heme *a* and Cu_A was limited by proton uptake on a 90 μs time scale. We have established the lower limit of the true rate constant for the electron transfer between Cu_A and heme *a* to be $\sim 2 \times 10^5$ s^{-1}.

Cytochrome *c* oxidase is a transmembrane enzyme located in the inner mitochondrial membrane. As the terminal member of the respiratory chain, it catalyzes the reduction of molecular oxygen to water by the soluble electron carrier, cytochrome *c* (*1*−*3*). On the matrix side of the membrane, four protons (scalar protons) are consumed for each oxygen molecule reduced. This reaction is coupled to the pumping of four additional protons (vectorial protons) from the matrix into the intermembrane space (*4*). The resultant proton gradient is the driving force for the generation of chemical energy in the form of ATP by the enzyme ATP synthase.

Although the electron transfer steps of the oxygen reaction have been investigated extensively by rapid spectroscopic techniques (*3*, *5*), studies on proton transfer have until recently been limited. Early flow-flash/single-wavelength detection measurements (*6*−*8*) indicated that proton transfer reactions were controlling the rates of electron transfer during the reduction of dioxygen to water, including the electron transfer between Cu_A[1] and heme *a*. More recently, on the basis of the crystal structures of cytochrome oxidase from bovine heart (*9*−*11*) and *Paracoccus denitrificans* (*12*, *13*), three possible proton conduction pathways, the D-, K-, and H-channels, have been proposed. Site-directed mutagenesis and spectroscopic studies on cytochrome oxidase from *P. denitrificans* and the bacterial oxidases from *Escherichia coli* and *Rhodobacter sphaeroides*, which have been assumed to have crystal structures similar to those of the *Paracoccus* oxidase and the bovine enzyme, have indicated that the K-channel might be important during the reduction of the

† This work was supported by National Institutes of Health Grant GM 537888.

* Corresponding author. E-mail: olof@chemistry.ucsc.edu. Fax: (831) 459-2935.

‡ Max-Planck-Institut for Biochemistry.

§ Dartmouth College.

|| University of California at Santa Cruz.

[1] Abbreviations: Cu_A, mixed-valence copper A center; Cu_B, copper B; HEPES, *N*-(2-hydroxyethyl)piperazine-*N*′-2-ethanesulfonic acid; MES, 2-(*N*-morpholino)ethanesulfonic acid; TAPS, *N*-tris(hydroxymethyl)methyl-3-aminopropanesulfonic acid; SVD, singular-value decomposition; TROA, time-resolved optical absorption; **P**, form of the enzyme in which heme a_3 has an absorbance maximum at ∼607 nm when referenced against its oxidized state; **F**, ferryl form of the enzyme in which heme a_3 has an absorbance maximum at ∼580 nm when referenced against its oxidized state; $\mathbf{F_o}$, **F** in which heme *a* is oxidized, one proton is at the binuclear center, and tyrosine is deprotonated; $\mathbf{F_I}$, **F** in which heme *a* is oxidized, one proton is at the binuclear center, and tyrosine is protonated; $\mathbf{F_{II}}$, **F** in which heme *a* is reduced, one proton is at the binuclear center, and tyrosine is protonated.

10.1021/bi981351h CCC: $18.00
Published on Web 02/17/1999

binuclear center (*14*−*21*). During the reaction of the reduced enzyme with O_2, both scalar and vectorial protons have been proposed to be taken up through the D-channel (*14*−*18*, *22*−*25*). Dynamic studies of proton uptake by residues on the protein surface have also shown that the proton-input side carries a proton-collecting antenna consisting of carboxylates and histidines (*16*, *26*).

In this study, we extended existing single-wavelength measurements of proton uptake in bovine cytochrome oxidase (*7*, *8*) by using time-resolved optical absorption (TROA) with multichannel detection. In addition to simultaneously monitoring a broad range of wavelengths, this method offers the advantage of high spectral resolution which greatly facilitates the identification of intermediates (*27*, *28*). Knowing the spectral shape of the intermediates becomes particularly valuable for deducing a reaction mechanism. Multichannel detection furthermore facilitates separation of spectral changes due to the redox centers from those of the pH indicator. This allowed us to determine both the rates and stoichiometry of proton transfer events and to link them to electron transfer steps occurring during oxidation of the solubilized, fully reduced enzyme. We have also established the lower limit of the true electron transfer rate between Cu_A and heme *a*. On the basis of these results, a mechanism incorporating both electron and proton transfer events is proposed.

MATERIALS AND METHODS

Materials. Cytochrome *c* oxidase was isolated from bovine hearts according to the procedure described by Yoshikawa et al. (*29*). To minimize the buffering capacity of the sample, the enzyme was repeatedly dialyzed against a buffer composed of 75 mM potassium sulfate and 80 μM buffer (MES was used for measurements at pH 6.5, HEPES at pH 7.5, and TAPS at pH 8.5) before being used. All chemicals were analytical grade and were used without further purification.

Flow-Flash Measurements. Fully reduced cytochrome *c* oxidase (30−40 μM) was prepared by addition of sodium ascorbate (5 mM) and hexammineruthenium(II) chloride (12.5 μM) under anaerobic conditions. The sample was then incubated for 30 min, while being stirred occasionally, under an atmosphere containing 20% carbon monoxide and 80% nitrogen, which resulted in the formation of CO-bound fully reduced cytochrome *c* oxidase. The pH of the sample was measured anaerobically with a needle electrode and adjusted, if necessary, by adding small aliquots of degassed potassium hydroxide or sulfuric acid. Formation of the fully reduced and the fully reduced CO-bound species was confirmed spectroscopically in the Soret and visible regions.

The reaction of fully reduced oxidase with oxygen was followed using the flow-flash technique (*30*). In a flow cell (80 μL), fully reduced CO-bound oxidase was mixed with an equal amount of oxygen-saturated buffer that contained 75 mM potassium sulfate and 80 μM phenol red (pH 7.5). The reaction was initiated 450 ms after mixing by photolyzing the CO complex with a laser pulse (Nd:Yag laser, λ = 532 nm, 65 mJ/pulse) and probed after various delay times with a gated (20 ns gate) multichannel detector using a xenon flash lamp (*31*). Fifty transient difference spectra were recorded at delay times between 50 ns and 50 ms that were equally spaced on a logarithmic scale. Each spectrum was generated by averaging the signals of 15 consecutive runs. All measurements were performed at 25 °C.

To separate spectral changes related to proton transfer from those due to ligand binding and redox events, a second set of measurements in the absence of the indicator, but under otherwise identical conditions, was performed. In this case, the pH indicator in the oxygen solution was replaced with 80 μM HEPES.

When measurements were conducted at a pH different from 7.5, phenol red was replaced in the oxygen-saturated buffer with the pH indicators carboxyfluorescein (pH 6.5, 40 μM) and *m*-cresol purple (pH 8.5, 80 μM). Furthermore, HEPES was substituted with 80 μM MES (pH 6.5) or 80 μM TAPS (pH 8.5).

Calibration of the Dye Response. Immediately after a flow-flash experiment, a small sample (1 mL) of the postreaction mixture was collected and transferred into an anaerobic cell filled with a gas mixture with the same composition as the atmosphere under which the fully reduced CO-bound enzyme had been prepared. Several aliquots (10 μL) of degassed 5 mM sodium hydroxide or 2.5 mM sulfuric acid were added, and the spectrum of the sample was recorded after each addition. After correction for dilution, the difference spectrum characterizing the response of the dye to the addition of 50 μM protons or hydroxide ions was obtained by direct subtraction.

Determination of the Buffering Capacity. One milliliter of a mixture containing 40 μM buffer and 40 μM pH indicator (the final concentrations of the buffer and dye in the flow-flash experiment) in 75 mM potassium sulfate was titrated with 10 μL aliquots of 5 mM sodium hydroxide, and the resultant changes in pH were monitored with a microelectrode. The buffering capacity of the solution at a given pH (β) was calculated as the extrapolated concentration of added hydroxide necessary to change the pH by 1 unit.

$$\beta = -\frac{d[H^+]}{d(pH)} = \frac{d[OH^-]}{d(pH)} \quad (1)$$

The buffering capacity of the enzyme solution was determined by an analogous titration of a 1 mL sample taken from the waste of a flow-flash experiment.

RESULTS

Spectral Changes Involving the Redox Centers. Figure 1 shows the transient spectra recorded in the presence and absence of a pH indicator dye (phenol red) at pH 7.5. There is a clear difference between the two sets in the region around 550 nm, the absorbance maximum of the phenol red indicator. To separate the dye signal from spectral changes originating from ligand and redox events, the spectral changes associated with the redox centers must be identified. To accomplish this, the data matrix containing the 50 transient spectra recorded in the absence of pH indicator (Figure 1B) was subjected to singular value decomposition (SVD). The first 10 singular values together with the first 10 columns of the **U** and **V** matrixes sufficiently represented the original data matrix, and only these were used for further analysis (*32*).

The SVD analysis was followed by multiexponential fitting. An adequate fit was achieved with a minimum of

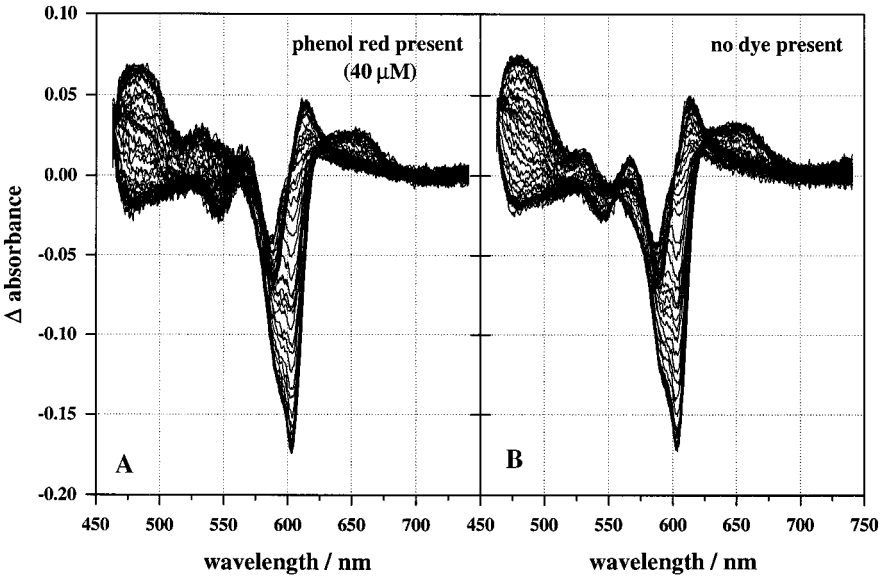

FIGURE 1: Fifty transient absorption spectra collected between 50 ns and 50 ms at delay times that were equally spaced on a logarithmic scale: (A) 40 μM phenol red present and (B) no dye present. The spectra were referenced against the fully reduced CO-bound enzyme and measured at pH 7.5 in a buffer containing 75 mM potassium sulfate and 40 μM HEPES. Each spectrum represents the average of 15 repeats. The concentration of the reacting enzyme was 9.5 μM, and the oxygen concentration after mixing was 650 μM.

Table 1: Apparent Lifetimes at Three pH Values Resulting from a Five-Exponential Fit[a]

	pH 6.5		pH 7.5		pH 8.5	
step	lifetime	H^+/enzyme	lifetime	H^+/enzyme	lifetime	H^+/enzyme
1	0.8 ± 0.3 μs	−	0.9 ± 0.4 μs	−	1.4 ± 0.6 μs	−
2	10 ± 5 μs	−	10 ± 5 μs	−	13 ± 5 μs	−
3	29 ± 5 μs	−	36 ± 5 μs	−	37 ± 5 μs	−
4	90 ± 25 μs	0.8 ± 0.3	90 ± 25 μs	0.6 ± 0.2	250 ± 70 μs	0.9 ± 0.5
5	1.1 ± 0.1 ms	0.4 ± 0.3	1.3 ± 0.1 ms	0.8 ± 0.2	2.2 ± 0.2 ms	0.7 ± 0.5

[a] Proton uptake stoichiometries linked to the slowest electron transfer events were the results of the double-exponential fits displayed in Figure 3.

five kinetic processes that yielded five *b* spectra (spectral changes associated with the apparent rate constants). At pH 7.5, for example, the data could be satisfactorily fitted with the following five apparent lifetimes: 0.93 μs, 10 μs, 36 μs, 90 μs, and 1.3 ms. The residuals (the difference between the data and the fit) had a random structure (not shown) and a noise level comparable to that of the experiment. The values of the determined lifetimes agreed with previous observations (*27*, *28*, *33*) and implied the existence of six intermediates.

A summary of all the apparent lifetimes observed at the three pH values is given in Table 1. The error intervals in the apparent lifetimes were estimated from experiment-to-experiment variation rather than from error analysis of each data set. It indicates that the apparent lifetimes observed at pH 6.5 were identical to those seen at pH 7.5 within experimental error. Analysis of data collected at pH 8.5 showed no significant changes in the lifetimes of the three fastest processes within the experimental error. The two slower rates, however, were notably affected by the pH increase with their lifetimes increasing by a factor of about 2 (250 μs and 2.2 ms).

Spectral Changes Due to Proton Transfer. To separate the dye signal from the spectral changes caused by the redox centers, we assumed that each transient spectrum recorded in the presence of the pH indicator could be expressed as a sum of a transient spectrum recorded in the absence of a pH indicator and a spectral contribution from the dye. This assumption is the basis for the following equation:

$$a(\lambda) = f_1 a_1(\lambda) + f_2 a_2(\lambda) + f_3 \quad (2)$$

where a represents a transient spectrum recorded in the presence of the dye, a_1 is the corresponding transient spectrum collected after the same delay time but in the absence of the dye, and a_2 is the spectral change of the dye in response to addition of a defined amount of protons or hydroxide ions as obtained from the calibration procedure described above. For each delay time, a least-squares fitting routine was employed to find the set of parameters (f_1, f_2, and f_3) that minimized the difference between the two sides of eq 2.

The parameter f_1 takes into account the fact that the photolytic yield of the reaction was somewhat lowered by the presence of the dyes phenol red and *m*-cresol purple which absorbed some of the photolyzing laser light. In these cases, the values for f_1 were found to be slightly smaller than 1. When carboxyfluorescein was used, f_1 could be set equal to 1 for all delay times because this dye does not absorb near 532 nm. The parameter f_2 quantifies the contribution of the dye signal to the overall spectrum, and f_3 eliminates a possible baseline shift between a pair of transient spectra. For experiments with phenol red and *m*-cresol purple, the entire wavelength range between 450 and 750 nm was used for the fitting. In the case of carboxyfluorescein, points above

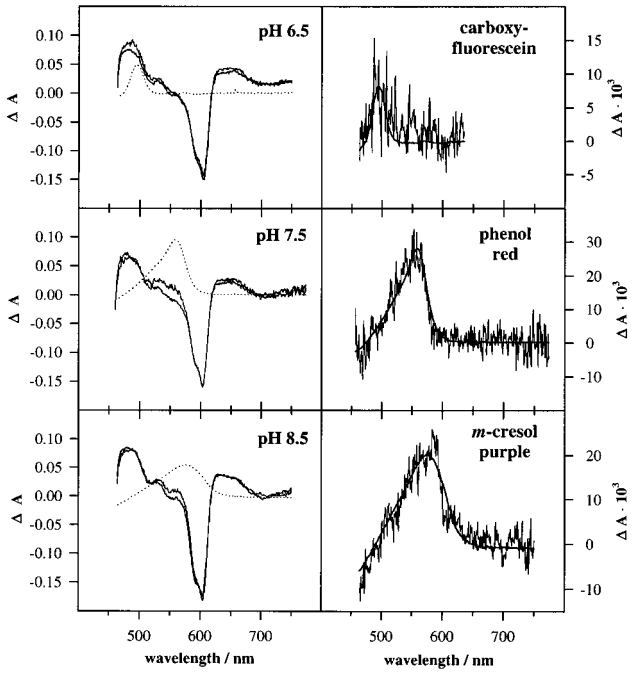

FIGURE 2: Extraction of the dye signals. (Left panels) Pairs of transient absorption spectra recorded in the presence (upper curves) and absence (lower curves) of a pH indicator after a delay time of 3 ms at pH 6.5 (top panel), 7.5 (middle panel), and 8.5 (bottom panel). The dotted lines represent the spectral response of the dyes to the addition of 50 μM sodium hydroxide (carboxyfluorescein at pH 6.5, phenol red at pH 7.5, and *m*-cresol purple at pH 8.5). (Right panels) Comparison of the calibrated dye signals (smooth lines) and the difference between the spectra recorded in the presence and absence of the dye, corrected, when appropriate, for different photolytic yields and baseline shifts.

550 nm were excluded because the dye had no notable absorbance in this region. Figure 2 (left panels, solid lines) shows the transient spectra recorded with a 3 ms delay in the presence (upper curves) and absence (lower curves) of a pH indicator at three pH values. The dotted line represents the spectral response of the dyes to the addition of 50 μM sodium hydroxide. Figure 2 (right panels) shows the differences between the transient spectra in the presence and absence of the dye, including, when appropriate, corrections for different photolytic yields and baseline shifts. The shapes of these difference spectra accurately match the profiles of the calibrated dye spectra (Figure 2, right panels, smooth solid lines). The figure also reveals that at their peaks, the difference spectra are clearly distinguishable and significantly larger than the noise level.

The parameter relevant for proton transfer is f_2, which quantifies the contribution of the dye signal to the overall spectrum. Graphs of f_2 versus time in Figure 3 show *when* proton transfer occurs and establishes *how many* protons per enzyme are involved. Clearly, the most prominent feature of these plots is a sharp increase indicative of proton uptake which starts around 50 μs and is essentially complete in the early millisecond range. The graphs furthermore suggest that the proton uptake occurs in two steps whose lifetimes appear to coincide with the two slowest electron transfer events in the enzyme (*27*, *28*). No faster proton transfer processes with amplitudes above the noise level could be identified unambiguously. We therefore fitted the data to a double-exponential rise with fixed rate constants (those of the two slowest electron transfer events) but variable amplitudes. Because the response time of the system was limited by the time required for protons to diffuse from the enzyme to the dye (see below), only delay times longer than 1 μs were included in the fit. For all three pH values, the experimental data were accurately described by the fits (Figure 3). The results of the fitting are summarized in Table 1. Fitting routines that used both amplitudes *and* lifetimes as adjustable fitting parameters produced the same results within experimental error.

The net stoichiometry of the proton uptake totaled about 1.3 ± 0.3 protons per enzyme at pH 6.5, 1.4 ± 0.2 at pH 7.5, and 1.6 ± 0.5 at pH 8.5. Within experimental error, it was split about equally between the two consecutive steps (Table 1).

An alternative approach for identifying which electron transfer steps are linked to proton transfer is illustrated in Figure 4 for data at pH 7.5. After singular value decomposition, the data set in the presence of a pH indicator (Figure 4, left panels, solid lines) and in its absence (Figure 4, left panels, dotted lines) was subjected to multiexponential fitting with common adjustable lifetimes. Differences in the resultant *b* spectra that could be attributed to the pH indicator (Figure 4, right panels) were extracted by a fitting procedure equivalent to that described by eq 2. The *b* spectra corresponding to the three fastest processes are basically congruent (Figure 4A−C, left panels) and do not permit the extraction of a dye signal of significant size (Figure 4A−C, right panels). However, the differences in the *b* spectra for the two slowest steps clearly indicate proton uptake (Figure 4D,E), confirming our earlier assignment of proton transfer to these events.

Electron Transfer between Cu_A and heme a. We have attempted to establish the true rate constant for the electron transfer between Cu_A and heme *a*. Figure 5 (a and b, ○) shows the time courses (on a logarithmic scale) of the reaction of the fully reduced enzyme with dioxygen at 606 and 446 nm, at the absorption maxima of the reduced heme *a*. The data were extracted from multichannel time-resolved experiments in the visible and Soret regions (*28*). The solid lines overlaying the experimental curves are the results of a five-exponential fit to the data using lifetimes similar to those reported here and in our earlier studies (*28*). As expected from the good correspondence between the experimental spectra and model spectra of the postulated intermediates (this study and ref *28*), there is an excellent agreement between the experimental curve and the fit at both wavelengths. Figure 5 (c and d, ○) shows an expanded view of the time course between 20 μs and 2 ms. The other curves represent a six-exponential fit to the data, including a variable (2−100 μs) additional lifetime for the reversible conversion of $\mathbf{F_I}$ to $\mathbf{F_{II}}$, i.e., the electron transfer between Cu_A and heme *a*. The microscopic rate constants of the forward and backward processes exhibited a ratio of 2:1 to account for the concentration ratio of the two ferryl forms. Including the sixth lifetime resulted in the same apparent lifetimes for the other processes as obtained for the five-exponential fit, but the apparent lifetime for the last step ($\mathbf{F_{II}} \rightarrow \mathbf{H}$) was decreased from 1.3 to 0.9 ms to yield good agreement between the experimental and theoretical curves. It is clear that at both 606 and 446 nm lifetimes longer than ~5 μs do not fit the data, and the best fit is obtained with a lifetime equal to or less than 2−5 μs. Analogous results were obtained when the data were analyzed at 415 nm.

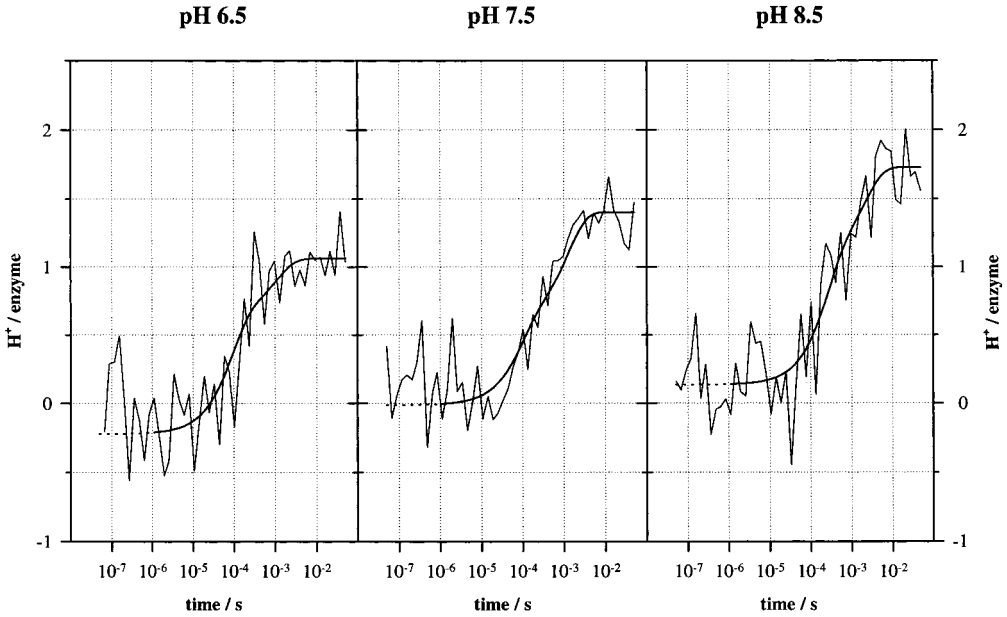

FIGURE 3: Proton transfer as a function of time as calculated from parameter f_2 at three different pH values (see the text for details). The smooth lines represent a double-exponential fit (see Table 1 for amplitudes) to the data using the rate constants of the two slowest redox events. The dotted lines show the extrapolation of the fitted curves into the range of early delay times (<1 μs) that was not included in the fitting.

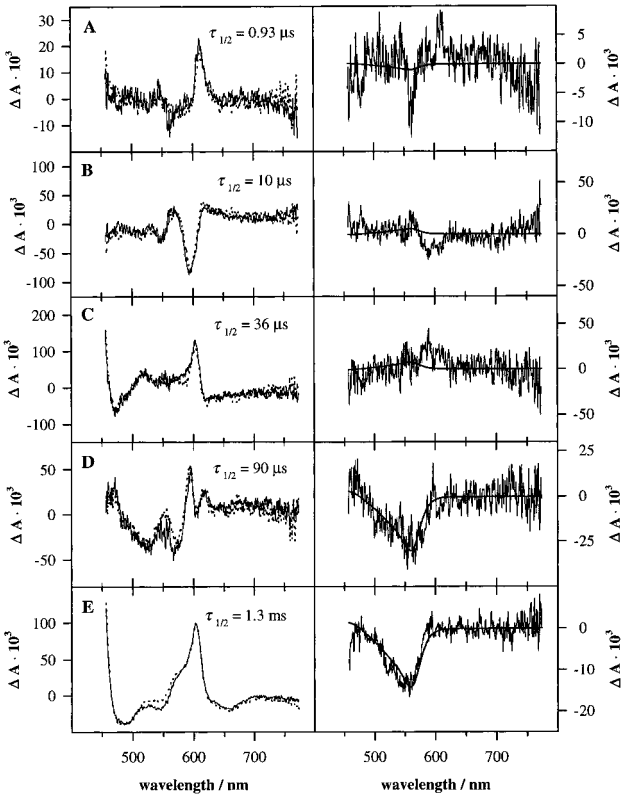

FIGURE 4: Analysis of *b* spectra for a potential dye component (phenol red at pH 7.5). (Left panels) *b* spectra resulting from data collected in the presence (solid lines) and absence of phenol red (dotted lines) in the order of increasing lifetimes (shortest on top). (Right panels) *b* spectra from data recorded in the presence of phenol red after subtracting the spectral contributions of redox centers and baseline shifts. The smooth lines depict the best possible fit of the calibrated dye spectrum to the difference spectra.

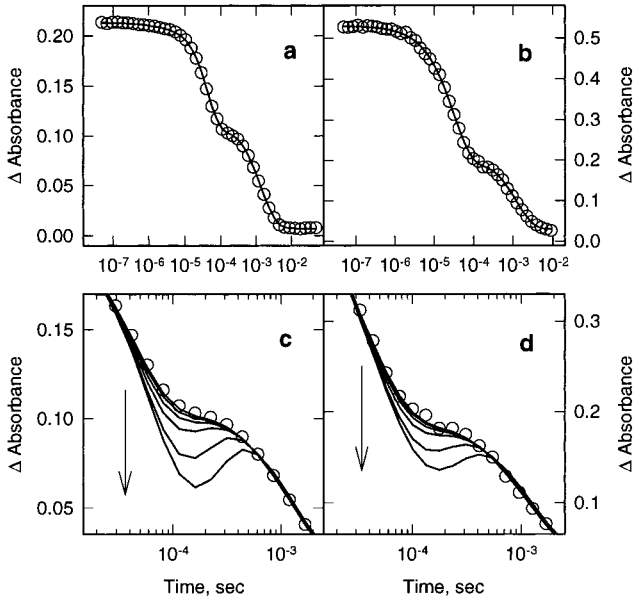

FIGURE 5: Panels a and b show the time courses (on a logarithmic scale) of the reaction of the fully reduced enzyme with dioxygen at 606 and 446 nm, respectively. The experimental data (○) were extracted from multichannel time-resolved experiments in the visible and Soret regions (*28*). The solid lines overlaying the experimental points are the results of a five-exponential fit to the data using lifetimes from our earlier studies (*28*) which are similar to those reported here. Panels c and d show an expanded view of the time course between 20 μs and 2 ms at 606 and 446 nm, respectively. The solid curves represent a six-exponential fit to the data, including a variable (2−100 μs) additional lifetime for the reversible conversion of $\mathbf{F_I}$ to $\mathbf{F_{II}}$, i.e., the electron transfer between Cu_A and heme *a*. The sixth lifetime was 100, 50, 20, 10, 5, and 2 μs, and the arrow indicates the direction of increasing lifetime.

DISCUSSION

In this study, we used time-resolved multichannel detection experiments in conjunction with dyes to investigate the coupled kinetics of electron and proton transfer events in cytochrome *c* oxidase. Our results provide an important first confirmation of previous observations on proton uptake obtained by single-wavelength measurements (*6*−*8*). Furthermore, we have shown that the higher spectral resolution

Scheme 1: Proposed Mechanism for the Reduction of Molecular Oxygen to Water by Cytochrome *c* Oxidase[a]

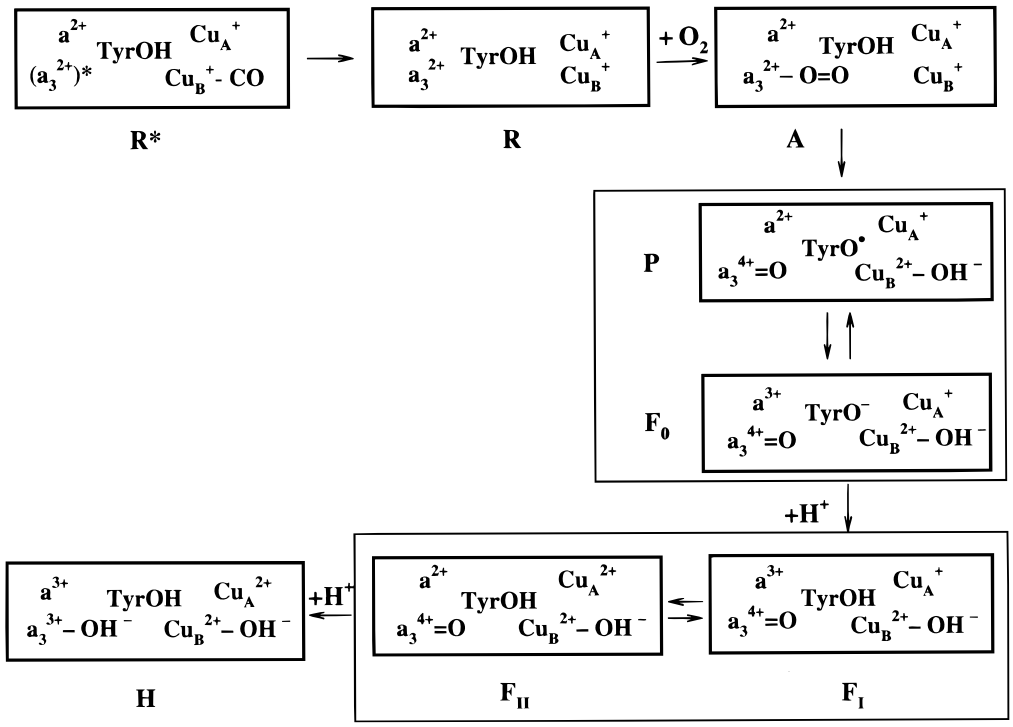

[a] Tyrosine 244, represented here as TyrOH, is postulated to function as an H-atom donor during the cleavage of the O−O bond (**A** → **P**).

Table 2: Rate Constants Obtained at pH 7.5 from Kinetic Modeling According to Scheme 1[a]

reaction	*k*	reaction	*k*
R* → **R**	$1.1 \times 10^6\ s^{-1}$	$\mathbf{P/F_o} \rightarrow \mathbf{F_I/F_{II}}$	$1.1 \times 10^4\ s^{-1}$
R → **A**	$1.5 \times 10^8\ M^{-1}\ s^{-1}$	$\mathbf{F_I/F_{II}} \rightarrow \mathbf{H}$	$7.4 \times 10^2\ s^{-1}$
A → $\mathbf{P/F_o}$	$2.8 \times 10^4\ s^{-1}$		

[a] The rate constant for the back reaction in the reversible **R*** → **R** step (*34*) was negligibly small and therefore omitted (see the text for details).

of the multichannel method permits extraction of spectral changes arising from pH-sensitive dyes which strongly overlap the oxidase spectral features and are up to 1 order of magnitude lower in intensity than the spectral shifts associated with the redox states of the enzyme. On the basis of our multichannel data and mechanistic analysis, we have also determined the upper limit of the true electron transfer rate constant between heme *a* and Cu_A.

Spectral Changes Involving the Enzyme Redox Centers. To interpret the apparent lifetimes and their corresponding *b* spectra on a mechanistic level, a kinetic model is required. Scheme 1 shows our recently proposed mechanism for oxygen reduction which is consistent with data both from the visible and Soret regions (*28*). On the basis of this kinetic model, we extracted the spectra of the postulated intermediates (referenced vs the oxidized enzyme) which were similar to our recently published spectra (*28*). Good agreement was observed between model spectra postulated by the mechanism and the experimental spectra, providing further support for the proposed mechanism. The model spectra were constructed by linear combination of reference spectra as described elsewhere (*27*, *28*). A summary of the rate constants employed for the kinetic modeling at pH 7.5 is given in Table 2.

The form of the enzyme generated immediately after photolysis (**R***) is a species having carbon monoxide bound to Cu_B, with heme a_3 in a conformation different from that of the fully reduced enzyme. In the first step of the mechanism (Scheme 1), carbon monoxide dissociates from Cu_B. Simultaneously, there is a relaxation of heme a_3, and as a result, the fully reduced cytochrome *c* oxidase (**R**) is formed (*34*). This reaction is complete in the early microsecond range. Previous studies have shown that the equilibrium constant for the first step ($K = k_{on}/k_{off}$) is $\sim 90\ M^{-1}$ (*31*, *34*). In our experiments, the conditional equilibrium constant ($K_{cond} = K[CO]$) equals 9.1×10^{-3}, implying that the contribution of the back rate is negligible.

The first step is followed by the coordination of dioxygen to heme a_3. The binding occurs with a lifetime of approximately 10 μs and leads to the formation of the ferrous−oxy compound (**A**). So far, no redox chemistry has taken place.

According to recent electron transfer results from both the visible and Soret regions (*28*), compound **A** decays into **P** which is rapidly converted to $\mathbf{F_o}$. The interconversion between **P** and $\mathbf{F_o}$ is significantly faster than the decay of compound **A**, and therefore, a mixture of **P** and $\mathbf{F_o}$ is observed (*28*). In **P** and $\mathbf{F_o}$, heme a_3 has absorbance maxima at 607 and 580 nm, respectively, when referenced versus oxidized heme a_3. In **P**, heme *a* is reduced, while it is oxidized in $\mathbf{F_o}$. To achieve a good fit, we modeled this intermediate with a 1:1 mixture of **P** and $\mathbf{F_o}$, in agreement with our previous model (*28*). The structure of **P** is under debate, and a peroxy structure, $a_3^{3+}-O^--O^-$ (*27*, *35*), and a ferryl structure, $a_3^{4+}=O$, in which an amino acid provides the extra oxidizing equivalent, have been proposed (*15*, *28*, *36*). Recent time-resolved resonance Raman experiments have provided strong support for the O−O bond being broken in the 607 nm species (*37*, *38*). In Scheme 1, the 607 nm

species is proposed to be a_3^{4+}=O Cu_B^{2+}−OH^- with the oxidizing equivalent on tyrosine 244 which also serves as a proton donor. Tyrosine 244 has recently been shown to be cross-linked to His 240, which is a ligand to Cu_B (*11*, *13*). The hydroxyl group of tyrosine 244 is situated close enough to the binuclear center to form a hydrogen bond with the O_2 ligand bound to the reduced heme a_3 (*11*, *38*). In $\mathbf{F_o}$, heme a_3 is also in a ferryl state (a_3^{4+}=O), while heme *a* has donated an electron to the tyrosine radical. The formation of **P** and the transfer of the third electron to form the $\mathbf{F_o}$ species are equivalent to the formation of compounds I and II of peroxidases, respectively (*17*, *39*, *40*).

In the fourth step (apparent lifetime of ∼90 μs), the mixture of **P** and $\mathbf{F_o}$ decays into $\mathbf{F_I}$, followed by rapid electron transfer between Cu_A and heme *a* forming $\mathbf{F_{II}}$. A transfer of one proton from the bulk medium on a 90 μs time scale is consistent with our proton uptake results, and we propose that tyrosinate picks up the proton to produce a tyrosine. The electron redistribution between Cu_A and heme *a* takes place at a rate faster than the formation of $\mathbf{F_I}$ (see below), and the rapid interconversion between the two ferryl-species is the reason for observing a mixture of $\mathbf{F_I}$ and $\mathbf{F_{II}}$. The fitting implied that about 66% of the heme *a* is reduced ($\mathbf{F_{II}}$) and 33% oxidized ($\mathbf{F_I}$), in agreement with our previous results (*28*).

The last step in the scheme involves the transfer of one electron from heme *a* to heme a_3. This process is characterized by an apparent lifetime in the early millisecond range. A concurrent uptake of a second proton, which binds to the oxygen atom located at heme a_3, is proposed. The final product of this sequence is the ferric hydroxy form of the enzyme (**H**) with a hydroxide coordinated to the heme a_3 and to Cu_B. This step is analogous to the conversion of compound II to the ferric species in the catalytic cycle of peroxidases (*39*, *40*).

Only the last two steps in Scheme 1 displayed pH sensitivity. While the rate constants for the decay of the $\mathbf{P}/\mathbf{F_o}$ and $\mathbf{F_I}/\mathbf{F_{II}}$ mixtures were identical at pH 6.5 and 7.5 within experimental error, we observed a notable decrease by a factor of 2 at pH 8.5 for both processes (Table 1). These findings are consistent with earlier observations from single-wavelength measurements conducted at pH values between 6 and 9 (*8*, *33*). The pH dependence of these processes points to their involvement in proton transfer.

Proton Transfer Events. When proton transfer studies are performed with solubilized pH indicator molecules, it is important to know the minimum response time of the system to determine whether spectral changes in the dye are limited by the diffusion rate of protons from the enzyme to the dye. We therefore estimated the maximum time required for a proton to diffuse from an enzyme to an indicator molecule. At a dye concentration of 40 μM, the maximum distance between enzyme and indicator molecules, *x*, is approximately 3×10^{-8} m. This distance was calculated on the basis of the assumption that the dye molecules are homogeneously distributed throughout the solution and occupy the corners of a cubic lattice. The longest distance possible between an enzyme molecule and the closest dye molecule is then given by the distance between the center and the corners of such a cube. If the diffusion coefficient of protons (*D*) in the sample is known, one can calculate the time (*t*) necessary for a proton to diffuse along this distance according to the Einstein−Smoluchowski relation (*41*):

$$t = \frac{x^2}{6D} \tag{3}$$

As pointed out by Junge and McLaughlin (*42*), the apparent diffusion coefficient of protons in a buffered solution (D_{app}) containing mobile and fixed buffers (in this case, the enzyme functions as a much less mobile buffer) can be orders of magnitude lower than the diffusion coefficient of a free proton in pure water (see ref *43* for a review of proton transfer dynamics). If the buffering capacities of both mobile and fixed buffers in the system are known, D_{app} can be estimated as follows:

$$D_{app} \approx D_{H^+}\left(\frac{2.3[H^+]}{\beta_{tot}}\right) + D_{OH^-}\left(\frac{2.3[OH^-]}{\beta_{tot}}\right) + D_{mobile}\frac{\beta_{mobile}}{\beta_{tot}} + D_{fixed}\frac{\beta_{fixed}}{\beta_{tot}} \tag{4}$$

Here, the diffusion coefficient of protons in bulk water, D_{H^+}, was taken to be 9×10^{-5} cm^2/s (*42*) and the diffusion coefficient of hydroxide ions, D_{OH^-}, was assumed to be 2×10^{-5} cm^2/s. The diffusion coefficient of the mobile, organic buffers was approximated by 1×10^{-5} cm^2/s (*42*). Since the only fixed buffer in the system, the enzyme, has a very small diffusion coefficient of approximately 1×10^{-7} cm^2/s, a typical value for large proteins (*44*), its contribution to D_{app} never exceeded 10% of the final value. The total buffering capacity of the system, β_{tot} (8×10^{-4} M), was obtained with the titration experiments described above. The buffering capacity due to mobile buffers, β_{mobile}, of 10^{-4} M was the experimentally determined buffering capacity of a mixture composed of 40 μM organic buffer and 40 μM pH indicator. Under these conditions, the major contribution to D_{app} comes from the mobile buffer, regardless of pH. The value of D_{app} was calculated according to eq 4 to be 1.3×10^{-6} cm^2/s.

Consequently, we expect the system to be in equilibrium after about 1 μs (eq 3). This is considerably faster than steps 2−5 in Scheme 1 and about as fast as the lifetime of the first step in the sequence. Therefore, we conclude that the response time of the system is sufficiently fast to accurately detect potential proton transfer events if they occur simultaneously with all the processes of the enzyme reaction except the first one, the formation of the fully reduced enzyme.

In general, proton transfer events observed in the bulk phase during the oxidation of solubilized, fully reduced cytochrome *c* oxidase can be attributed to several causes. In the simplest case, protons disappearing from the bulk are scalar protons which are directly consumed at the active site, i.e., they participate in the reduction of dioxygen to water. Their transport to the binuclear center occurs without delay, and the rates of the electron transfer steps dictate the rate of proton disappearance from the bulk water.

Alternatively, the release or uptake of protons in the bulk can be initiated by Bohr effects which originate from structural rearrangements or charge redistributions initiated by redox events inside the enzyme (*11*, *45*). These events result in pK_a shifts of amino acid residues (*45*, *46*). Although

the Bohr effects are ultimately triggered by redox events in the active site, the location of proton release or binding may be far away from the metal centers, in which case the protons involved are unrelated to those required for the reduction of oxygen. It is possible that residues inside the proton channel connecting the bulk phase with the binuclear site, presumably the D-channel, are subject to Bohr effects. In this case, protons consumed at the active site could be donated by these side chains. Since the reprotonation of these residues by protons from the bulk phase may precede or follow proton consumption at the active site, these two events would not necessarily be synchronized.

Vectorial protons are another potential cause of pH changes in the bulk, provided that their uptake and release by the enzyme occur on significantly different time scales. This has been observed for the proton pump bacteriorhodopsin in purple membrane fragments, where proton release and the following uptake could be clearly distinguished (*47*, *48*). If, however, uptake and release of vectorial protons take place simultaneously, no pH changes in the bulk will be detected. In this case, only studies of systems in which the matrix and intermembrane surface of the oxidase are physically separated, such as the enzyme reconstituted in liposomes, can provide further information about pumped protons (*6*). Nilsson and co-workers have shown that during flash-induced oxidation of bovine cytochrome oxidase reconstituted into phospholipid vesicles proton release to the medium occurs with a rate constant of 9×10^2 s^{-1} (*6*), which is similar to that of the second phase of the proton uptake in the solubilized enzyme reported here and previously (*8*).

We observed a total uptake of 1.3−1.6 protons concurrently with the two slowest electron transfer events. In view of the errors in Table 1, there is no difference between the number of protons taken up at different pH values. The stoichiometries are essentially consistent with earlier experimental data (*7*, *8*) and electrostatic calculations based on the X-ray structure of the enzyme (*46*). Most likely, the uptake stoichiometry reflects the consumption of two scalar protons through the D-channel, which is counteracted to a small extent by the release of Bohr protons. The uptake of the third and fourth scalar protons must take place during the re-reduction of the enzyme, since these protons are not detected by the indicator in the bulk solution. This assumption is in good agreement with results of Mitchell and Rich (*49*) and Capitanio et al. (*45*), who have shown that two protons are taken up during the reduction of the binuclear center. Site-directed mutagenesis studies suggest that these protons are taken up through the K-channel (*14*, *15*, *17*−*21*). The concurrent uptake of two protons with the reduction of the binuclear center has been proposed to result from the requirements of electroneutrality (*50*).

The first proton is proposed to be taken up from tyrosine 244 (Scheme 1) during the cleavage of the oxygen−oxygen bond. Proton donation by an amino acid residue rather than the bulk medium could account for the lack of proton uptake observed on this time scale. In agreement with our results, Hallén and co-workers did not observe proton uptake or pH dependence for the 10 and 30 μs lifetimes (*8*). However, the 30 μs phase showed a kinetic isotope effect along with the 100 μs and 1 ms redox phases, which indicated the involvement of protons in these processes. On the basis of these results, it was postulated that the earliest proton uptake occurred during the 30 μs redox phase or, in our case, upon the decay of compound **A** to **P**.

Electron Transfer between Cu_A and Heme a. The reprotonation of the tyrosine residue by protons from the bulk is proposed to occur on a 100 μs time scale and forms intermediate $\mathbf{F_I}$. This is followed by a faster electron transfer between Cu_A and heme *a* forming $\mathbf{F_{II}}$. The rate of electron transfer between Cu_A and heme *a* has been suggested to be controlled by proton uptake (*8*, *51*−*53*), and our studies support these results. We have estimated the lower limit of the true apparent rate constant for the electron redistribution between Cu_A and heme *a* ($\mathbf{F_I} \rightarrow \mathbf{F_{II}}$) to be $\sim 2 \times 10^5$ s^{-1}. These results are in agreement with electrons transfer rates estimated from analysis of a tunneling pathway between Cu_A and heme *a* (*54*, *55*). The best Cu_A−heme *a* pathway starts from His 204, a ligand to one of the coppers in the dinuclear Cu_A center, and consists of 14 covalent bonds and two hydrogen bonds which amounts to an effective tunneling path of 25 Å. The estimated activation-less rate constant is $\sim 9 \times 10^5$ s^{-1} (*55*). With a driving force of ~90 meV, the value of the reorganization energy, λ, must be close to 0.3 eV to account for the fast rate (*55*, *56*). The proton transfer control of the electron transfer rate between Cu_A and heme *a* may reflect the importance of a tight coupling between the proton-pumping machinery and the electron transfers to the partially reduced oxygen intermediates that drive the pump (*5*).

It should be pointed out that our determination above of the true rate of electron transfer between Cu_A and heme *a* is based on the multichannel detection method. The analysis relies on our proposed reaction mechanism and the good agreement between experimental spectra and model spectra of the postulated intermediates (*28*), and it could not have been accomplished using single-wavelength detection. For example, the time course at 606 nm could satisfactorily be fitted using the 20 μs lifetime if the amplitude of the fourth intermediate (the mixture of **P** and $\mathbf{F_o}$) was increased. However, this would correspond to changing the extinction coefficient of intermediate 4 at 606 nm. Thus, if one redetermines the experimental intermediate spectra from the kinetic matrix (describing the mechanism) which includes the 20 μs lifetime, the experimental intermediate spectra, although matching the model spectra of the postulated intermediates at 606 nm, do not match the model spectra when they are compared over the whole wavelength range. However, an excellent fit is observed using an apparent sixth lifetime between 2 and 5 μs.

In the final step of Scheme 1, a second proton from the bulk binds to the oxygen atom at heme a_3 as the enzyme is converted from the ferryl mixture ($\mathbf{F_I}$/$\mathbf{F_{II}}$) to the oxidized ferric hydroxy (**H**) form. This is in good agreement with other reports (*7*, *8*). The final product is a species that has a hydroxide ion bound to Cu_B and to heme a_3.

REFERENCES

1. Wikström, M., Krab, K., and Saraste, M. (1981) in *Cytochrome Oxidase: A Synthesis*, Academic Press, New York.
2. Babcock, G. T., and Wikström, M. (1992) *Nature 356*, 301−309.
3. Einarsdóttir, Ó. (1995) *Biochim. Biophys. Acta 1229*, 129−147.
4. Wikström, M. (1977) *Nature 266*, 271−273.
5. Ferguson-Miller, S., and Babcock, G. T. (1996) *Chem. Rev. 96*, 2889−2907.

6. Nilsson, T., Hallén, S., and Oliveberg, M. (1990) *FEBS Lett. 260*, 45−47.
7. Oliveberg, M., Hallén, S., and Nilsson, T. (1991) *Biochemistry 30*, 436−440.
8. Hallén, S., and Nilsson, T. (1992) *Biochemistry 31*, 11853−11859.
9. Tsukihara, T., Aoyama, H., Yamashita, E., Tomizaki, T., Yamaguchi, H., Shinzawa-Itoh, K., Nakashima, R., Yaono, R., and Yoshikawa, S. (1995) *Science 269*, 1069−1074.
10. Tsukihara, T., Aoyama, H., Yamashita, E., Tomizaki, T., Yamaguchi, H., Shinzawa-Itoh, K., Nakashima, R., Yaono, R., and Yoshikawa, S. (1996) *Science 272*, 1136−1144.
11. Yoshikawa, S., Shinzawa-Itoh, K., Nakashima, R., Yaono, R., Yamashita, E., Inoue, N., Yao, M., Fei, M. J., Libeu, C. P., Mizushima, T., Yamaguchi, H., Tomizaki, T., and Tsukihara, T. (1998) *Science 280*, 1723−1729.
12. Iwata, S., Ostermeier, C., Ludwig, B., and Michel, H. (1995) *Nature 376*, 660−669.
13. Ostermeier, C., Harrenga, A., Ermler, U., and Michel, H. (1997) *Proc. Natl. Acad. Sci. U.S.A. 94*, 10547−10553.
14. Pfitzner, U., Odenwald, A., Ostermann, T., Weingard, L., Ludwig, B., and Richter, O.-M. H. (1998) *J. Bioenerg. Biomembr. 30*, 89−97.
15. Gennis, R. B. (1998) *Biochim. Biophys. Acta 1365*, 241−248.
16. Karpefors, M., Ädelroth, P., Aagaard, A., Sigurdson, H., Svensson Ek, M., and Brzezinski, P. (1998) *Biochim. Biophys. Acta 1365*, 159−169.
17. Vygodina, T. V., Pecoraro, C., Mitchell, D., Gennis, R. B., and Konstantinov, A. A. (1998) *Biochemistry 37*, 3053−3061.
18. Konstantinov, A. A., Siletsky, S., Mitchell, D., Kaulen, A., and Gennis, R. B. (1997) *Proc. Natl. Acad. Sci. U.S.A. 94*, 9085−9090.
19. Zaslavsky, D., and Gennis, R. B. (1998) *Biochemistry 37*, 3062−3067.
20. Jünemann, S., Meunier, B., Gennis, R. B., and Rich, P. R. (1997) *Biochemistry 36*, 14456−14464.
21. Ädelroth, P., Gennis, R. B., and Brzezinski, P. (1998) *Biochemistry 37*, 2470−2476.
22. Ädelroth, P., Svensson Ek, M., Mitchell, D. M., Gennis, R. B., and Brzezinski, P. (1997) *Biochemistry 36*, 13824−13829.
23. Watmough, N. J., Katsonouri, A., Little, R. H., Osborne, J. P., Furlong-Nickels, E., Gennis, R. B., Brittain, T., and Greenwood, C. (1997) *Biochemistry 36*, 13736−13742.
24. Verkhovskaya, M. L., Garcia-Horsman, A., Puustinen, A., Rigaud, J.-L., Morgan, J. E., Verkhovsky, M. I., and Wikström, M. (1997) *Proc. Natl. Acad. Sci. U.S.A. 94*, 10128−10131.
25. Brzezinski, P., and Ädelroth, P. (1998) *J. Bioenerg. Biomembr. 30*, 99−107.
26. Sacks, V., Marantz, Y., Aagaard, A., Checover, S., Nachliel, E., and Gutman, M. (1998) *Biochim. Biophys. Acta 1365*, 232−240.
27. Sucheta, A., Georgiadis, K. E., and Einarsdóttir, Ó. (1997) *Biochemistry 36*, 554−565.
28. Sucheta, A., Szundi, I., and Einarsdóttir, Ó. (1998) *Biochemistry 37*, 17905−17914.
29. Yoshikawa, S., Choc, M. G., O'Toole, M. C., and Caughey, W. S. (1977) *J. Biol. Chem. 252*, 5498−5508.
30. Gibson, Q. H., and Greenwood, C. (1963) *Biochem. J. 86*, 541−554.
31. Georgiadis, K. E., Jhon, N.-I., and Einarsdóttir, Ó. (1994) *Biochemistry 33*, 9245−9256.
32. Henry, E. R., and Hofrichter, J. (1992) *Methods Enzymol. 210*, 129−193.
33. Oliveberg, M., Brzezinski, P., and Malmström, B. G. (1989) *Biochim. Biophys. Acta 977*, 322−328.
34. Einarsdóttir, Ó., Dyer, R. B., Lemon, D. D., Killough, P. M., Hubig, S. M., Atherton, S. J., López-Garriga, J. J., Palmer, G., and Woodruff, W. H. (1993) *Biochemistry 32*, 12013−12024.
35. Morgan, J. E., Verkhovsky, M. I., and Wikström, M. (1996) *Biochemistry 35*, 12235−12240.
36. Weng, L., and Baker, G. M. (1991) *Biochemistry 30*, 5727−5733.
37. Proshlyakov, D. A., Ogura, T., Shinzawa-Itoh, K., Yoshikawa, S., Appelman, E. H., and Kitagawa, T. (1994) *J. Biol. Chem. 269*, 29385−29388.
38. Proshlyakov, D. A., Pressler, M. A., and Babcock, G. T. (1998) *Proc. Natl. Acad. Sci. U.S.A. 95*, 8020−8025.
39. English, A. M., and Tsaprailis, G. (1995) *Adv. Inorg. Chem. 43*, 79−125.
40. Konstantinov, A. A., Vygodina, T. V., Capitanio, N., and Papa, S. (1998) *Biochim. Biophys. Acta 1363*, 11−23.
41. Levine, I. N. (1995) in *Physical Chemistry*, Chapter 16, McGraw-Hill, New York.
42. Junge, W., and McLaughlin, S. (1987) *Biochim. Biophys. Acta 890*, 1−5.
43. Gutman, M., and Nachliel, E. (1990) *Biochim. Biophys. Acta 1015*, 391−414.
44. Smith, M. H. (1970) in *CRC Handbook of Biochemistry* (Sober, H. A., Ed.) Chapters 10−12, CRC Press, Cleveland, OH.
45. Capitanio, N., Vygodina, T. V., Capitanio, G., Konstantinov, A. A., Nicholls, P., and Papa, S. (1997) *Biochim. Biophys. Acta 1318*, 255−265.
46. Kannt, A., Lancaster, C. R. D., and Michel, H. (1998) *Biophys. J. 74*, 708−721.
47. Lozier, R. H., Niederberger, W., Bogomolni, R. A., Hwang, S., and Stoeckenius, W. (1976) *Biochim. Biophys. Acta 440*, 545−556.
48. Heberle, J., and Dencher, N. A. (1992) *Proc. Natl. Acad. Sci. U.S.A. 89*, 5996−6000.
49. Mitchell, R., and Rich, P. R. (1994) *Biochim. Biophys. Acta 1186*, 19−26.
50. Rich, P. R., Meunier, B., Mitchell, R., and Moody, A. J. (1996) *Biochim. Biophys. Acta 1275*, 91−95.
51. Ädelroth, P., Svensson Ek, M., Mitchell, D. M., Gennis, R. B., and Brzezinski, P. (1997) *Biochemistry 36*, 13824−13829.
52. Hallén, S., and Brzezinski, P. (1994) *Biochim. Biophys. Acta 1184*, 207−218.
53. Svensson Ek, M., and Brzezinski, P. (1997) *Biochemistry 36*, 5425−5431.
54. Ramirez, B. E., Malmström, B. G., Winkler, J. R., and Gray, H. B. (1995) *Proc. Natl. Acad. Sci. U.S.A. 92*, 11949−11951.
55. Regan, J. J., Ramirez, B. E., Winkler, J. R., Gray, H. B., and Malmström, B. G. (1998) *J. Bioenerg. Biomembr. 30*, 35−40.
56. Brzezinski, P. (1996) *Biochemistry 35*, 5611−5615.

BI981351H